**COMPARISON OF CLEMENTINE LWIR AND UVVIS IMAGES: FACTORS CONTROLLING LUNAR SURFACE TEMPERATURES** S. L. Lawson and B. M. Jakosky, Laboratory for Atmospheric and Space Physics, University of Colorado, Boulder, CO 80309-0392 (lawson@argyre.colorado.edu).

**Introduction:** With the completion of the calibration of the Clementine long-wave infrared (LWIR) camera images [Lawson *et al.*, *JGR*, in press], the information can now be used in conjunction with other data sets to investigate lunar surface thermal behavior. In an effort to better understand the factors which control lunar surface temperatures, we compare an LWIR mosaic to images from the Clementine ultraviolet-visible (UVVIS) camera. The mare region being investigated is centered at 48˚N, 355.5˚E, which lies in the northern Mare Imbrium, just south of Montes Alpes. The LWIR and UVVIS mosaics can be seen in Figure 1. The LWIR image on the left extends approximately 1300 pixels north-south, while the 128 pixel east-west extent shows the width of the square camera frame. The resolution of this mosaic is approximately 69 meters per pixel. The UVVIS mosaic on the right of Figure 1 has a resolution of 100 meters per pixel and was created from the 750-nm basemap. Because the Clementine instruments were nadir-pointing, the phase angle $\alpha$ and incidence angle $i$ are essentially the same at approximately 48˚, while the emission angle $e$ is very close to 0˚.

Four regions of the two mosaics were analyzed. The regions are roughly outlined and labeled in Figure 1. For the cross plots shown in Figure 2, the regions defined in Figure 1 were individually co-registered. The plots in Figure 2 show LWIR temperature as a function of UVVIS reflectance factor, which is further discussed below. The UVVIS images were photometrically corrected to a standard viewing geometry of $i = \alpha = 30^\circ$ and $e = 0^\circ$.

**Analysis:** In an effort to understand the behavior of the cross-plots shown in Figure 2, we created a model which calculates the correlation between reflectance and temperature for a macroscopically rough surface with varying albedo. Our simple topographic model calculates the local variation of incidence and emission angles for the changing orientation of a surface element; given $i$, $e$, and $\alpha$ from the Clementine images, our topographic model finds the local $i'$ and $e'$ given a fixed $\alpha$. The model can be used to emulate either convex or concave topography; in this particular case we used it to help calculate the temperature and reflectance in the interior of a crater. Incorporating $i'$, $e'$, and $\alpha$, we simultaneously calculated the bidirectional reflectance and directional-hemispherical albedo.

The bidirectional reflectance can be found from

$$r(i',e',\alpha) = \frac{\omega}{4\pi}\frac{\mu_o}{\mu_o+\mu}\left[p(\alpha) + H(\mu_o)H(\mu) - 1\right]$$

where $\omega$ is the single-scattering albedo, $\mu_o = \cos i'$, $\mu = \cos e'$, $p(\alpha) = 1+b\cos\alpha$, $H(x) = (1+2x)/(1+2\gamma x)$, and $\gamma = (1-\omega)^{0.5}$. We have neglected the opposition effect. We found that $b = 1.4$ best fit Hapke's lunar photometric function for phase angles less than 90˚. We then corrected to a standard viewing geometry ($i = \alpha = 30^\circ$, $e = 0^\circ$) incorporating the McEwen photometric function that was used to calibrate the UVVIS images [LPSC XXVII, LPSC XXIX]. The model results are shown in terms of the reflectance factor, defined as the reflectance of the surface relative to a Lambertian surface under the same bidirectional illumination. We are calculating a broadband bidirectional reflectance, but the 750-nm data are single-wavelength measurements. We therefore incorporated a multiplicative factor into our model to adjust our broadband calculations to 750-nm.

The directional-hemispherical albedo, which determines the radiative equilibrium temperature, can be found from

$$r_h(i') = \frac{1-\gamma}{1+2\gamma\mu_o} + b\frac{\omega}{4}\frac{\mu_o}{1+2\mu_o}$$

where $i'$ are again our modeled crater incidence angles. If the Moon is assumed to be a smooth spherical object in instantaneous equilibrium with the solar insolation, then local temperature $T$ is calculated from

$$\varepsilon\sigma\frac{T^4}{\cos i'} = (1-r_h)\frac{S_o}{R^2}$$

with unit emissivity $\varepsilon$, Stefan-Boltzmann constant $\sigma$, solar constant $S_o$, and Sun-Moon distance $R$ in AU. The only free parameters in our modeling are the single-scattering albedo $\omega$ and the facet orientation.

**Discussion:** The black triangles in Figure 2 show the results of our topographic modeling: equilibrium temperature versus reflectance factor. We plot only those points that would lie inside a simple bowl-shaped crater. We have accounted for neither shadowing nor re-radiated thermal emission. The data from the four areas can be adequately fit with single-scattering albedos ranging from 0.29 to 0.39. The linear trend seen in the regions is a result of craters and is well fit by our model. The clustering of points, as particularly illustrated in region 3, is likely due to small variations in the single-scattering albedo of a flat surface. Region 2 is not well fit at high reflectances by one single-scattering albedo; as oppposed to the $\omega$ shown in Figure 2, $\omega = 0.49$ can be used to model high reflectance values. These different single-scattering albedos required to fit all of the data in region 3 may indicate a variation of single scattering albedo around the crater, or they may be indicative of other small-scale surface roughness effects not accounted for in our model. The equilibrium surface temperatures of the lunar surface shown in Figure 1 are well modeled by variations in macroscopic surface roughness and single-scattering albedo. Small-scale surface roughness likely plays a secondary role at this location.

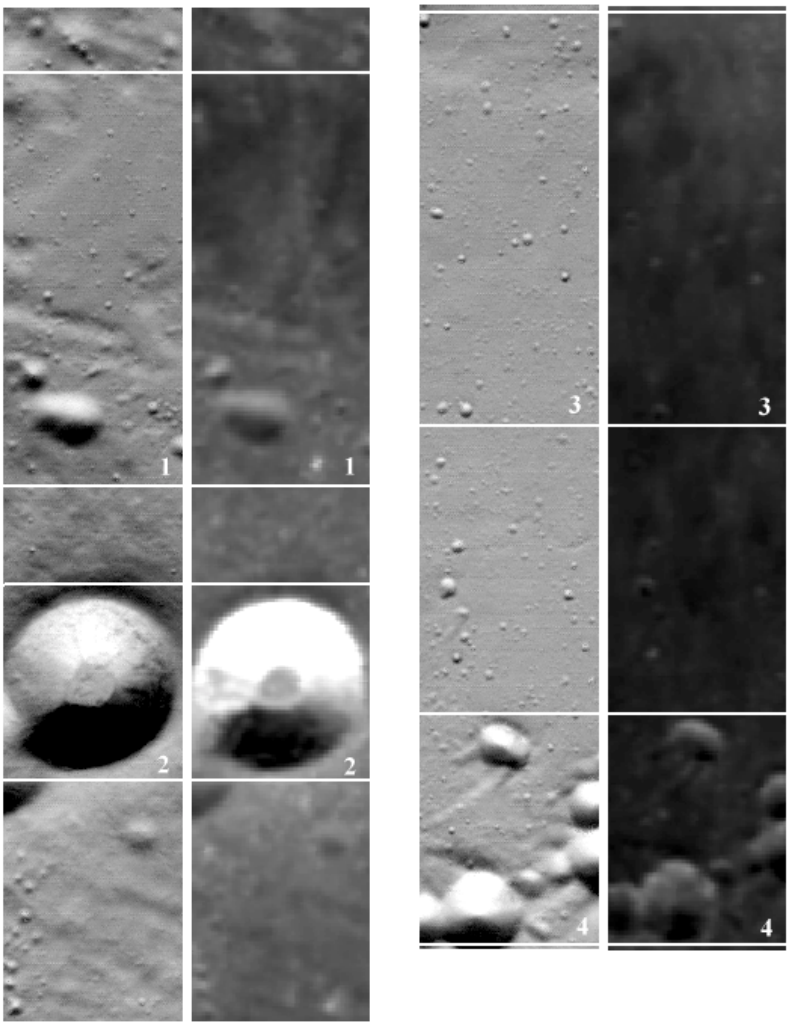


**Figure 1.** LWIR (left) and UVVIS (right) mosaics. The numbered regions are cross-plotted in Figure 2.

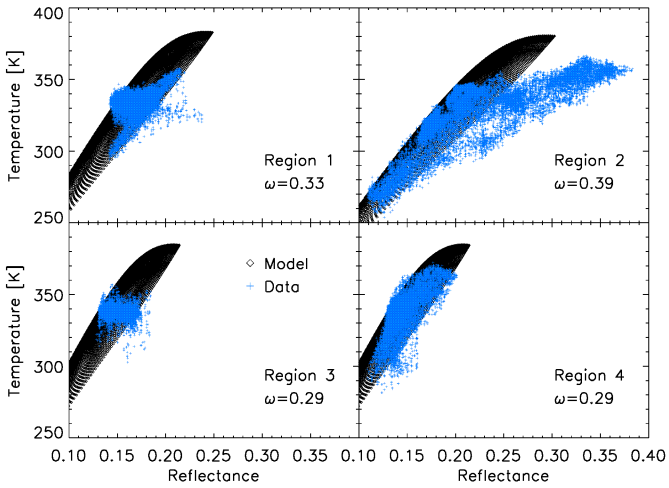


**Figure 2.** LWIR-derived temperature versus UVVIS 750-nm reflectance factor for the four regions outlined in Figure 1. The blue pluses represent the data and the black diamonds illustrate the model.